Intrinsic polarization switching in $BaTiO_3$ crystal under uniaxial electromechanical loading

Yingwei Li,[1,2,*] Jie Wang,[3,†] and Faxin Li[2,‡]

[1]*School of Civil Engineering and State Key Laboratory of Water Resources and Hydropower Engineering Science, Wuhan University, 430072 Wuhan, China*

[2]*State Key Laboratory for Turbulence and Complex Systems, College of Engineering, Peking University, Beijing 100871, China*

[3]*Department of Engineering Mechanics, School of Aeronautics and Astronautics, Zhejiang University, Hangzhou 310027, China*

(Received 13 June 2016; revised manuscript received 8 October 2016; published 21 November 2016)

Both 180° and 90° intrinsic polarization switching (IPS) in $BaTiO_3$ crystal were investigated by Landau-Ginzburg-Devonshire (LGD) theory under combined electric field and stress loading. Results show that for 180° PS, the coercive electric field ($E_{IC}^{180^\circ}$) increases under tension but decreases under compression with increasing stresses. The 90° PS was classified into two types. For type I 90° PS, $E_{IC}^{\mathrm{I}(90^\circ)}$ increases under tension but decreases under compression with increasing stresses, similar to 180° PS; while for type II 90° PS, an opposite variation trend is observed. (The definition of the type I and the type II 90° PS is given in the text.) Additionally, the calculation demonstrates that under tensile stresses or under compressive stresses between −140 and 0 MPa, the electric field needed to drive both types of 90° PS is smaller than that needed for driving 180° PS, implying that 180° PS is favorable to accomplish by two-step 90° PS. As E_{IC} refers to 180° PS in the past investigations, these demonstrate that the E_{IC} calculated by others may be overestimated. Moreover, the coercive stresses needed to drive 90° ferroelastic IPS was also calculated as a function of preloading bias electric fields.

DOI: 10.1103/PhysRevB.94.184108

I. INTRODUCTION

Polarization switching (PS) in ferroelectrics is a very complicated inhomogeneous process, which normally includes three stages: (i) nucleation of domains, in which the unit cells have different polarization directions compared to their initial state; (ii) forward growth; and (iii) sideways motion of the new formed domains [1–5]. However, such nucleation and domain wall motion dominated processes are not the only way of PS. Landau and Lifshitz pointed out that simultaneous reversal of all local dipoles without involving domain walls is also possible [6,7]. This type of PS was usually called intrinsic polarization switching (IPS) or "Landau switching" [8]. In general, the magnitude of the electric fields required to drive IPS (E_{IC}) is two to three orders higher than the coercive electric fields observed (E_C) in experiment. This situation is very similar to the paradox found by Landauer in 1957 [9]. He analyzed the domain nucleation processes in $BaTiO_3$ crystal, and found that even if a nucleus with reversed polarization direction can come into existence under low electric field, with the help of some localized effects such as defects and surface charges, the newly formed domains are not free to expand.

This discrepancy between E_C and E_{IC} has puzzled ferroelectricians for many years. Recently, along with the development of technologies on fabricating ultrathin ferroelectric films as well as the advancements in experimental apparatus, some investigations concerning IPS resurfaced. Bune *et al.* [10] fabricated ultrathin vinylidene fluoride copolymer films by Langmuir-Blodgett (LB) deposition, and then they measured the polarization response of these films. Results show that when the thickness of LB polymer films is below 15 nm, the measured E_C is in good agreement with the calculated E_{IC}. Based on the experimental results, they stated that they realized IPS in LB polymer films. However, this statement had been questioned on different grounds by others [11,12]. At present, the large E_C observed in their experiment is thought to be induced by the presence of a conductive nonferroelectric layer at the film-electrode interface [13]. Recently, by applying chemical potential rather than electric field, Highland *et al.* [14] stated they realized domain-free polarization switching in a 4.9-nm-thick $PbTiO_3$ film. But later they found that a stable nonpolar phase can exist between the positive and the negative polar states when varying the external chemical potential [15], implying that PS induced by chemical potential is quite different from that caused by electric field. In addition, some attempts were also conducted by others [16–19]; however, IPS in ferroelectrics is still yet to be realized experimentally [8].

It should be noted that in the past investigations, E_{IC} refers to 180° PS. However, in practicality, besides 180° PS, non-180° PS also exists [20]. Taking $BaTiO_3$ as an example, at room temperature, it is in tetrahedral phase and has six equivalent variants [Fig. 1(a)] [20]. Figure 1(b) shows its Gibbs free energy (ΔG) profile at 25 °C. The potential wells (point A, point B, point C, and point D) represent the possible existing variants. The value of the polarizations where the potential wells exist means the spontaneous polarization (P_0). When we apply proper electric fields along the P_3 direction, $-P_3$ can switch to $P_1/-P_1$ or $P_2/-P_2$ along the road of $A \rightarrow B$ or $A \rightarrow D$ by 90° PS (hereafter this type of 90° PS is referred to as type I 90° IPS); additionally, $P_1/-P_1$ and $P_2/-P_2$ can switch to P_3 along the road of $D \rightarrow C$ and $B \rightarrow C$ by 90° PS (hereafter this type of 90° PS is referred to as type II 90° IPS). Furthermore, our recent investigation demonstrated that the electric fields needed to drive the type II 90° PS are significantly smaller than that needed for driving 180° PS. However, the type I 90° PS was not investigated in that work [19]. So here comes a question: if we applied electric fields antiparallel to the polarization direction of ferroelectrics, can 180° PS be accomplished by two-step 90° PS along the

*Corresponding author: yingweili@whu.edu.cn
†Corresponding author: jw@zju.edu.cn
‡Corresponding author: lifaxin@pku.edu.cn

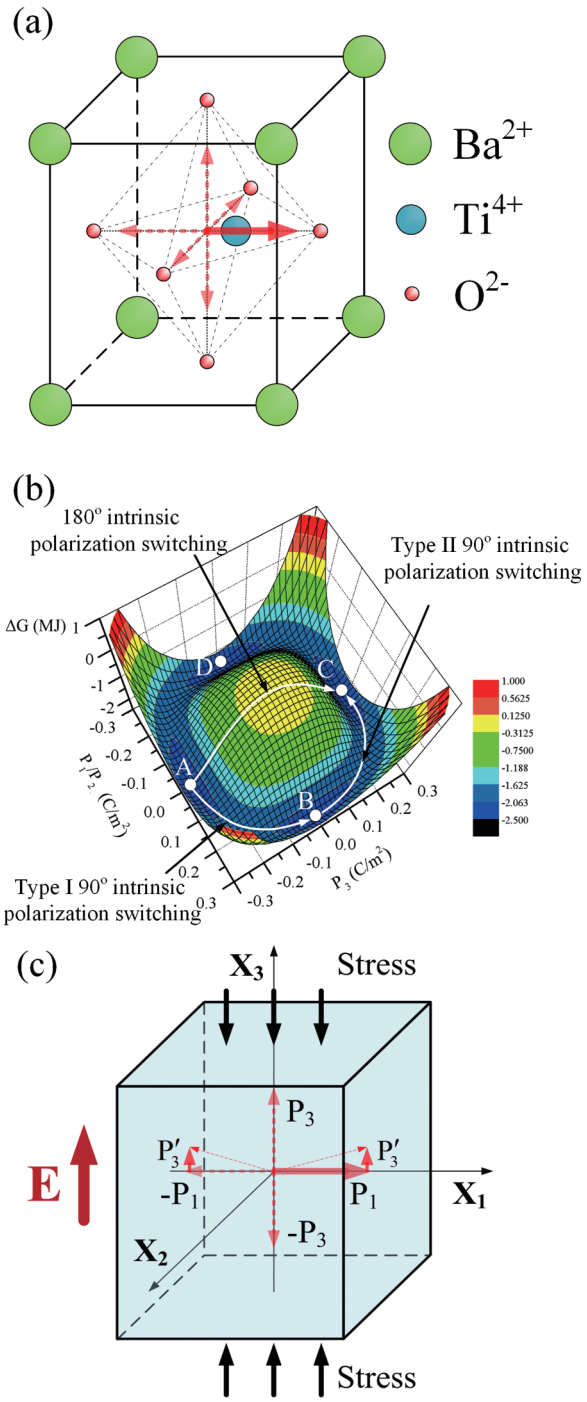

FIG. 1. (a) Crystal structure of $BaTiO_3$ crystal in tetragonal phase. The solid red arrow line represents the polarization state; the dashed red arrow lines represent the equivalent possible polarization state. (b) The Gibbs free energy profile of $BaTiO_3$ crystal at 25 °C. (c) Illustration of loading condition. Under electric field loading, P_1 and $-P_1$ will rotate along the electric field direction, and therefore P_3' appears. For simplicity, P_2 and $-P_2$ were not plotted out.

road of $A \rightarrow B \rightarrow C$ or $A \rightarrow D \rightarrow C$ instead of the road of $A \rightarrow C$? Motivated by this question, in this work, both 180° and 90° PS in $BaTiO_3$ were investigated by Landau-Ginzburg-Devonshire (LGD) theory under uniaxial electromechanical loading [Fig. 1(c)]. Results show that under tensile stresses or under compressive stresses between −140 and 0 MPa, the electric field needed to drive both types of 90° PS is smaller than that needed for 180° IPS, implying that 180°PS is favorable to accomplish by two-step 90° PS. In addition, the coercive stresses needed to drive 90° PS were also calculated.

II. LANDAU DEVONSHIRE THERMODYNAMICS POTENTIAL

Using the cubic paraelectric phase as the reference, the free energy of $BaTiO_3$ crystal as a function of polarization and stress can be written as [6]

$$\begin{aligned} f_{\mathrm{LGD}} = {} & \alpha_1\left(P_1^2+P_2^2+P_3^2\right)+\alpha_{11}\left(P_1^4+P_2^4+P_3^4\right) \\ & +\alpha_{12}\left(P_1^2P_2^2+P_2^2P_3^2+P_1^2P_3^2\right) \\ & +\alpha_{111}\left(P_1^6+P_2^6+P_3^6\right)+\alpha_{112}\left[P_1^4\left(P_2^2+P_3^2\right)\right. \\ & \left.+P_2^4\left(P_1^2+P_3^2\right)+P_3^4\left(P_1^2+P_2^2\right)\right]+\alpha_{123}P_1^2P_2^2P_3^2, \end{aligned} \tag{1}$$

where P_1, P_2, and P_3 mean the polarizations; α_{12}, α_{111}, α_{112}, and α_{123} are constant coefficients; α_1 and α_{11} are temperature dependent, which are $3.3(T-110)\times 10^5$ and $3.6(T-175)\times 10^6$(V m C^{-1}), respectively. Under electromechanical loading, instead of f_{LGD}, we should consider the Gibbs free energy

$$\begin{aligned} \Delta G = {} & f_{\mathrm{LGD}}-\tfrac{1}{2}s_{11}\left(\sigma_1^2+\sigma_2^2+\sigma_3^2\right) \\ & -\tfrac{1}{2}s_{12}(\sigma_1\sigma_2+\sigma_2\sigma_3+\sigma_3\sigma_1)-\tfrac{1}{2}s_{44}\left(\sigma_4^2+\sigma_5^2+\sigma_6^2\right) \\ & -Q_{11}\left(\sigma_1P_1^2+\sigma_2P_2^2+\sigma_3P_3^2\right) \\ & -Q_{12}\left[\sigma_1\left(P_2^2+P_3^2\right)+\sigma_2\left(P_1^2+P_3^2\right)+\sigma_3\left(P_1^2+P_2^2\right)\right] \\ & -Q_{44}(\sigma_4P_2P_3+\sigma_5P_1P_3+\sigma_6P_1P_2) \\ & -E_1P_1-E_2P_2-E_3P_3. \end{aligned} \tag{2}$$

Here σ_1, σ_2, σ_3, σ_4, σ_5, and σ_6 represent the applied stresses; E_1, E_2, and E_3 are the applied electric field; s_{11}, s_{12}, and s_{44} mean the elastic compliance constants of $BaTiO_3$ crystal in the cubic phase and Q_{11}, Q_{12}, and Q_{44} are the corresponding electrostrictive coefficients. The value of the coefficients mentioned above is given in Table I. In the following discussions, $-\frac{1}{2}s_{11}(\sigma_1^2+\sigma_2^2+\sigma_3^2)-\frac{1}{2}s_{12}(\sigma_1\sigma_2+\sigma_2\sigma_3+\sigma_3\sigma_1)-\frac{1}{2}s_{12}(\sigma_4^2+\sigma_5^2+\sigma_6^2)$ was ignored, as we focus on PS in ferroelectrics and this part does not influence the PS process.

III. RESULTS AND DISCUSSIONS

For 180° PS, the expression of the Gibbs free energy can be written as $\Delta G=\alpha_1P_3^2+\alpha_{11}P_3^4+\alpha_{111}P_3^6-Q_{11}\sigma_3P_3^2-E_3P_3$. Figure 2(a) illustrates the Gibbs free energy versus polarization curves of $BaTiO_3$ crystal under different electric fields without or with compressive stresses of −100 MPa. When we applied electric fields along the P_3 direction, the left part of the ΔG versus polarization curves lifts but the right part declines with increasing electric field. Simultaneously, the potential wells evolve with the change of the applied electric field. When the electric field reaches 15.8 MV/mm, the left potential well becomes unstable. The electric field at which the left potential well becomes unstable is called the

TABLE I. Values of the normalized coefficients of $BaTiO_3$ crystal at 25 °C [21].

α_1	α_{11}	α_{12}	α_{111}	α_{112}	α_{123}	s_{11}	s_{12}	s_{44}	Q_{11}	Q_{12}	Q_{44}
-0.2805×10^7	-5.4×10^8	4.9×10^8	6.6×10^9	2.9×10^9	3.678×10^{10}	8.3×10^{-12}	-2.7×10^{-12}	9.24×10^{-12}	0.11	−0.043	0.059
$Vm\,C^{-1}$	$Vm^5\,C^{-3}$	$Vm^5\,C^{-3}$	$Vm^9\,C^{-5}$	$Vm^9\,C^{-5}$	$Vm^9\,C^{-5}$	$m^2\,N^{-1}$	$m^2\,N^{-1}$	$m^2\,N^{-1}$	$m^4\,C^{-2}$	$m^4\,C^{-2}$	$m^4\,C^{-2}$

180° intrinsic coercive electric field ($E_{IC}^{180^\circ}$). With compressive stresses of −100 MPa, all the ΔG versus polarization curves lift, demonstrating the polarization state of ferroelectrics can be influenced by stresses. Simultaneously, $E_{IC}^{180^\circ}$ decreases from 15.8 to 11.6 MV/mm.

Similarly, if a negative electric field was applied, the right potential wall would become unstable when the electric field reaches $-E_{IC}^{180^\circ}$. Consequently, under a cyclic electric field loading, $BaTiO_3$ crystal shows electric field versus polarization (E-P) loops. Figure 2(b) shows the calculated E-P loops of $BaTiO_3$ crystal under various preloading compressive stresses, from which we can see that $E_{IC}^{180^\circ}$ increases under tension but decreases under compression with increasing stresses. Here it should be noted that in this part we only considered 180° PS, and did not think about the possibility of 90° PS. However, in fact, the compressive stress can induce 90° PS when the stresses reach −224 MPa. Such 90° PS has been observed in phase field modeling by Wu *et al.* [22] and will also be discussed later in this paper.

For 90° PS, Eq. (2) should be used. Figure 3 shows the Gibbs free energy profile of $BaTiO_3$ crystal under electric fields of 2.9, 15.2, and 15.8 MV/m. When the electric field reaches 2.9 MV/m, potential wells of B and D become unstable, demonstrating the type II 90° IPS happened. When the electric fields increase to 15.2 MV/m, the potential well of A becomes a saddle point. Although $-P_3$ cannot switch to P_3 along the road of $A \rightarrow C$, it can switch to P_3 along the road of $A \rightarrow B \rightarrow C$ or $A \rightarrow D \rightarrow C$. When the electric field increases to $E_{IC}^{180^\circ}$ (15.8 MV/m), $-P_3$ switches to P_3 along the road of $A \rightarrow C$, implying 180° PS can happen.

Figures 4(a) and 4(b) show the evolution of polarizations as a function of electric field without, and with compressive stresses of −50 MPa, respectively. Different from 180° PS, P_1 and $-P_1$ will rotate along the electric field direction, and therefore P_3' appears. The definition of P_3' is given in Fig. 1(b). (As P_2 and $-P_2$ overlap with P_1 and $-P_1$, P_2 and $-P_2$ were not plotted out in Figs. 4(a) and 4(b). By comparing Figs. 4(a) and 4(b), it can be seen that the electric field needed to drive both types of 90° IPS can be significantly influenced by stresses. With compressive stresses of −50 MPa, $E_{IC}^{\mathrm{I}\,(90^\circ)}$ decreases from 15.2 to 12.7 MV/m. For $E_{IC}^{\mathrm{II}\,(90^\circ)}$, it increases from 2.9 to 4.2 MV/m.

Figure 4(c) shows the calculated $E_{IC}^{\mathrm{I}\,(90^\circ)}$ and $E_{IC}^{\mathrm{II}\,(90^\circ)}$ under different stresses. For comparison, the evolution of $E_{IC}^{180^\circ}$ as a function of stresses was also plotted out. It can be seen that under tension, $E_{IC}^{\mathrm{I}\,(90^\circ)}$ increases but $E_{IC}^{\mathrm{II}\,(90^\circ)}$ decreases with increasing stresses. Under compression, an opposite variation trend is observed for $E_{IC}^{\mathrm{I}\,(90^\circ)}$ and $E_{IC}^{\mathrm{II}\,(90^\circ)}$. Furthermore, the figure demonstrates that under tensile stresses or under compressive stresses between −140 and 0 MPa, both $E_{IC}^{\mathrm{I}\,(90^\circ)}$ and $E_{IC}^{\mathrm{II}\,(90^\circ)}$ are smaller than $E_{IC}^{180^\circ}$, implying that 180° are favorable to accomplish by two-step 90° PS. As E_{IC} refers to 180° PS in the past investigations, these demonstrate that the $E_{IC}^{180^\circ}$ calculated by others may be overestimated.

In fact, some experimental results have revealed that in some situations, 180° PS is achieved by two-step 90° PS in ferroelectrics during electric field loading. For instance, Jiang *et al.* [23] and Li *et al.* [24] *in situ* investigated 180° PS in $BaTiO_3$ crystal, and found that under antiparallel electric field

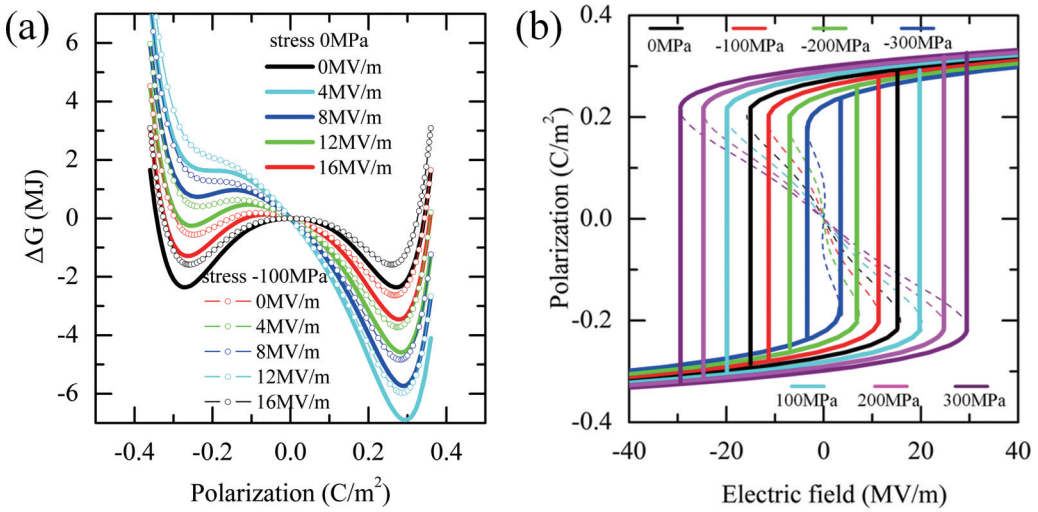

FIG. 2. (a) The Gibbs free energy of $BaTiO_3$ crystal under combined stress and electric field loading. The solid curves and symbol lines represent the Gibbs free energy versus polarization curves under different electric fields without or with preloading compressive stresses of −100 MPa, respectively. (b) The electric field versus polarization (E-P) loops of $BaTiO_3$ crystal under different preloading stresses.

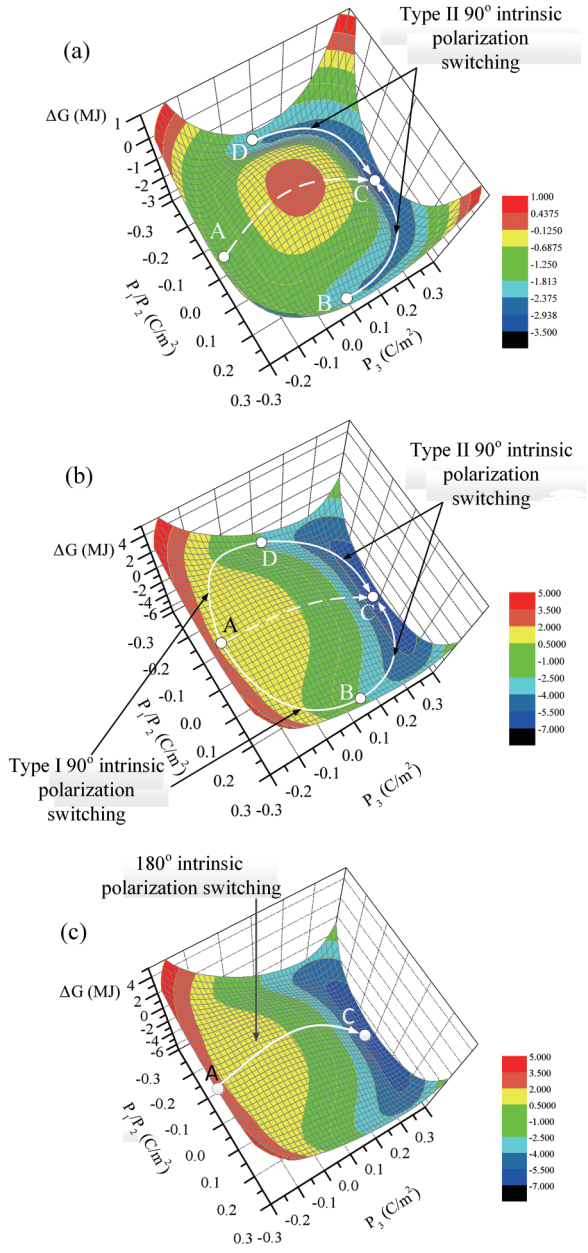

FIG. 3. The Gibbs free energy profile of $BaTiO_3$ crystal under different electric fields: (a) 2.9 MV/m, (b) 15.2 MV/m, and (c) 15.8 MV/m.

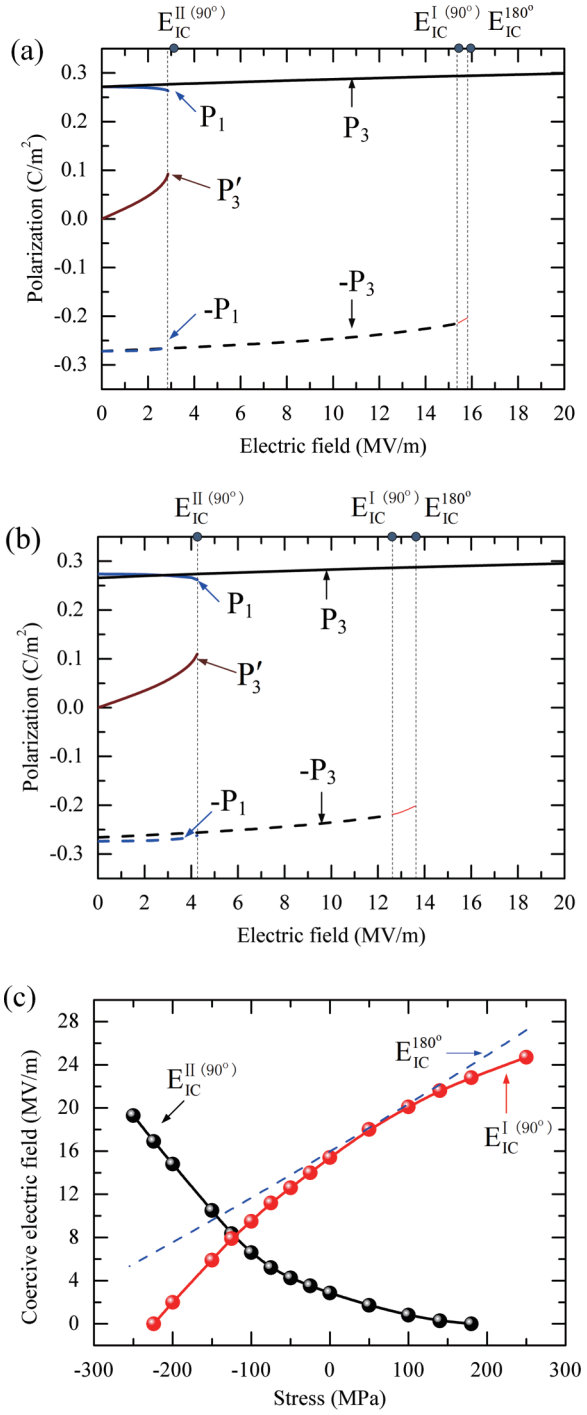

FIG. 4. The evolution of polarization in $BaTiO_3$ crystal as a function of electric field (a) without and (b) with compressive stresses of −50 MPa. (c) The evolution of a coercive field in $BaTiO_3$ crystal as a function of stresses.

loading, 180° PS was accomplished by two-step 90° domain switching, except in a perfectly poled specimen. Additionally, the electric field versus strain curves of Lead Zirconate Titanate (PZT) ceramics always show two long tails under certain cyclic electric field loading, demonstrating that a large amount of non-180° PS happened [25,26].

Different from 180° PS, 90° PS can also be induced by pure stress loading. Figures 5(a) and 5(b) show the Gibbs free energy profile of $BaTiO_3$ crystal under compressive stresses and tensile stresses of −224 and 180 MPa, respectively. When the compressive stresses reach −224 MPa, potential wells of *A* or *C* become unstable, and can switch to *B* or *D* by 90° PS. That is why $E_{IC}^{\mathrm{I}\,(90^\circ)}$ decreases to zero at compressive stresses of −224 MPa [Fig. 4(c)]. (In the following, this type of 90° PS will be named as type I 90° ferroelastic IPS). Similarly, the potential wells of *B* or *D* become unstable when the tensile stresses reach 180 MPa. As a result, $E_{IC}^{\mathrm{II}\,(90^\circ)}$ decreases to zero when the tensile stresses reach 180 MPa (this type of 90° PS will be named as type II 90° ferroelastic IPS).

Additionally, the stresses needed to drive the 90° ferroelastic PS can be influenced by electric fields. Figures 6(a)

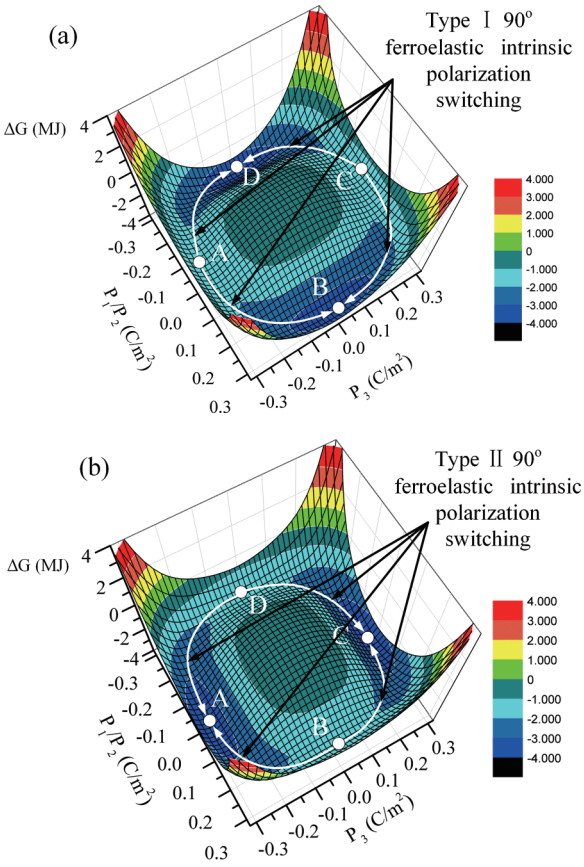

FIG. 5. The Gibbs free energy profile of $BaTiO_3$ crystal (a) under compressive stresses of −224 MPa and (b) under tensile stresses of 180 MPa.

and 6(b) show the polarizations of $BaTiO_3$ under different stresses without and with preloading electric fields of 2 MV/m, respectively. It can be seen that with preloading an electric field of 2 MV/m, the stresses needed to drive $P_1/-P_1$ to P_3 ($\sigma^{\mathrm{II}\,(90^\circ)}_{IC(P_1/-P_1\to P_3)}$) decreases from 180 to 40 MPa; the stresses needed to drive $-P_3$ to P_1 or $-P_1$($\sigma^{\mathrm{I}\,(90^\circ)}_{IC(-P_3\to P_1/-P_1)}$) decreases from −224 to −200 MPa; the stresses needed to drive P_3 to P_1 or $-P_1$ ($\sigma^{\mathrm{I}\,(90^\circ)}_{IC(P_3\to P_1/-P_1)}$) increases from −224 to −250 MPa.

Figure 6(c) shows the evolution of σ_{IC} as a function of preloading electric fields. For $\sigma^{\mathrm{II}\,(90^\circ)}_{IC(P_1/-P_1\to P_3)}$, it decreases with increasing electric fields. When the electric field reaches 2.8 MV/m, $\sigma^{\mathrm{II}\,(90^\circ)}_{IC(P_1/-P_1\to P_3)}$ decreases to zero. This is because when the electric field reaches 2.8 MV/m, the potential wells of B or D become unstable, and can be driven to the potential wells of A or C by an electric field [Fig. 4(c)]. For $\sigma^{\mathrm{I}\,(90^\circ)}_{IC(-P_3\to P_1/-P_1)}$, it increases with increasing the electric field. When the electric field increases to 15.2 MV/m, $\sigma^{\mathrm{I}\,(90^\circ)}_{IC(-P_3\to P_1/-P_1)}$ increases to zero, as P_3 can be driven to P_1 or $-P_1$ by electric fields; while for $\sigma^{\mathrm{I}\,(90^\circ)}_{IC(P_3\to P_1/-P_1)}$, it decreases with increasing the preloading electric field.

It should be noted that the Gibbs free energy of Eq. (2) excludes the gradient-related domain wall energy and the depolarization energy for inhomogeneous polarization distribution in ferroelectric materials. However, in practicality, the PS process is inevitably inhomogeneous [27]. In order to

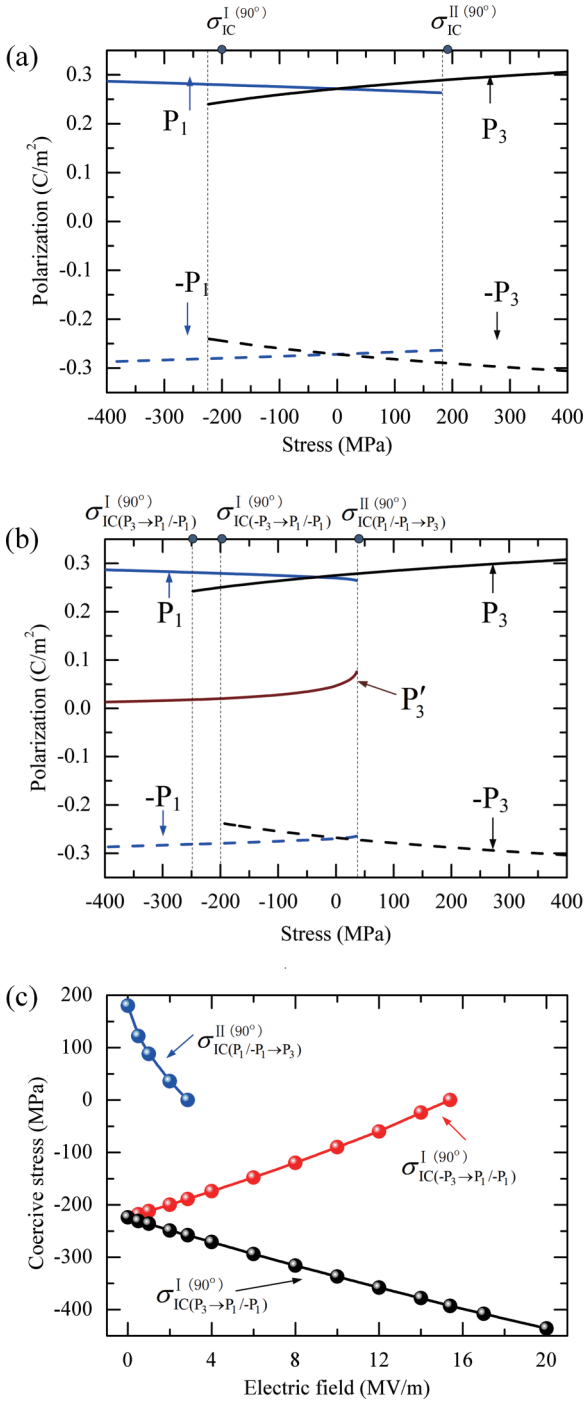

FIG. 6. The evolution of polarizations in $BaTiO_3$ crystal (a) under pure mechanical loading and (b) with preloading electric fields of 2 MV/m. (c) The evolution of coercive stress of $BaTiO_3$ crystal as a function of electric fields.

investigate the effect of domain wall [28–30] and depolarization energy [31] on the polarization switching behavior, as an example, we conduct phase field simulations on the 180° PS in a $BaTiO_3$ partial with dimension of 20 nm × 20 nm × 16 nm under different preloading compressive stresses. In the phase field model, the domain wall energy is included and described

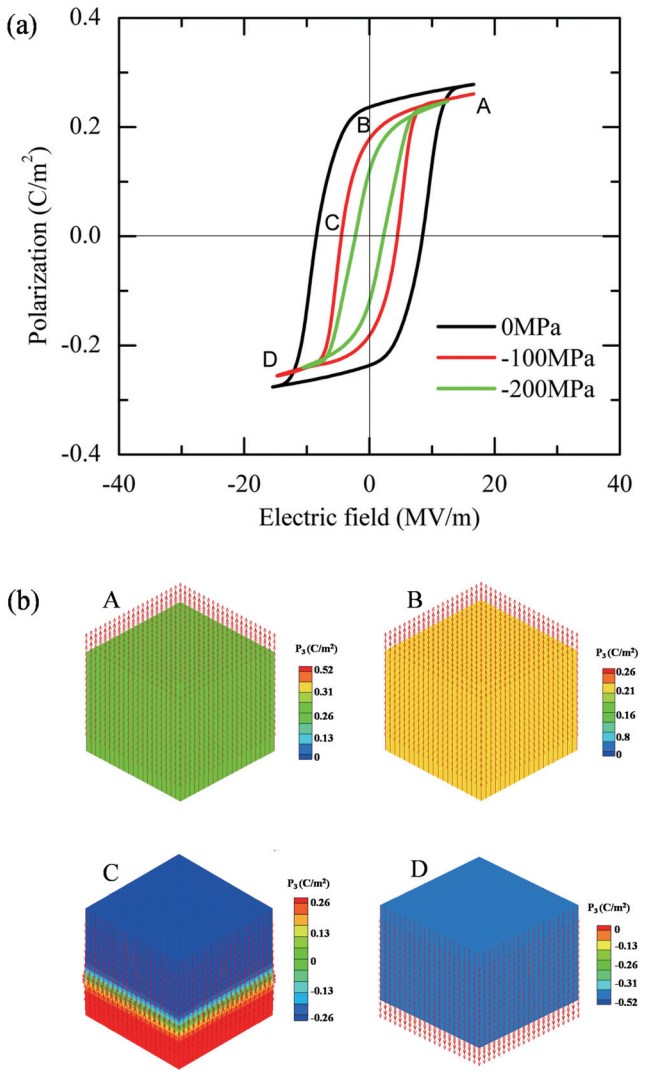

FIG. 7. (a) Electric field versus polarization curves simulated by a phase field model under different preloading compressive stresses. (b) Domain structure evolution process in $BaTiO_3$ crystal under electric field loading with compressive stress of −100 MPa.

as a function of polarization gradient,

$$f_{\text{grad}} = \tfrac{1}{2}G_{11}\left(P_{1,1}^2 + P_{2,2}^2 + P_{3,3}^2\right) + G_{12}(P_{1,1}P_{2,2} + P_{2,2}P_{3,3} + P_{1,1}P_{3,3}) + \tfrac{1}{2}G_{44}[(P_{1,2} + P_{2,1})^2 + (P_{2,3} + P_{3,2})^2 + (P_{1,3} + P_{3,1})^2] + \tfrac{1}{2}G'_{44}[(P_{1,2} - P_{2,1})^2 + (P_{2,3} - P_{3,2})^2 + (P_{1,3} - P_{3,1})^2], \quad (3)$$

where G_{11}, G_{12}, G_{44}, and G'_{44} are the gradient energy coefficients. For $BaTiO_3$, $G_{11} = 2.76 \times 10^{-10}$, $G_{12} = 0$, $G_{44} = G'_{44} = 1.38 \times 10^{-10}(\text{m}^4\,\text{N}\,\text{C}^{-2})$ are employed in the present study [17]. The depolarization energy is included in the phase field model by the self-consistent calculation of internal electric fields in the Gibbs free energy of Eq. (2) based on Maxwell's equations $D_{i,i} = 0$ $(i = 1,2,3)$. The stresses are self-consistently calculated from the mechanical equilibrium equations of $\sigma_{ij,j} = 0$ $(i,j = 1,2,3)$. The total energy includes the Gibbs free energy of Eq. (2) and the domain wall energy of Eq. (3). In the phase field model, the temporal evolution of spatially inhomogeneous polarization can be obtained by minimizing the total free energy, which is described by the following time-dependent Ginzburg-Landau (TDGL) equation,

$$\frac{\partial P_i(r,t)}{\partial t} = -L\frac{\delta F}{\delta P_i(r,t)} \quad (i = 1,2,3), \quad (4)$$

where L is the kinetic coefficient, and $F = \int_V (\Delta G + f_{\text{grad}})dv$ is the total free energy of the simulated system. The variation of $\delta F/\delta P_i(r,t)$ at the right-hand side of Eq. (4) represents the thermodynamic driving force for the spatial and temporal evolution of polarization, $r = (x_1,x_2,x_3)$ denotes the spatial vector, and t is time. The mechanical equilibrium equations, Maxwell's equations, and TDGL equations are solved by the finite element method, in which an eight-node brick element with seven degrees of freedom at each node is employed for the space discretization, and the backward Euler iteration method is adopted for the time integration [17].

Figure 7 shows the results of phase field simulations on the 180° PS under different preloading compressive stresses. The calculated coercive electric fields were 8.6 MV/m (0 MPa), 4.5 MV/m (−100 MPa), and 2.5 MV/m (−200 MPa), which were slightly smaller than the coercive electric fields calculated by Eq. (2). This demonstrates that the depolarization fields and the contribution of polarization gradient have influences on the PS behavior in ferroelectrics, but are not critically important. Additionally, at 90° PS, the changes of spontaneous deformation can create significant difficulty in the scenario of polarization reversal. For instance, the real sample is either a ceramic plate or a thin epitaxial film. In such cases either the interaction of individual ceramic grains or adhesion to the substrate will hinder the 90° reorientation. However, as a primary work, we consider the 90° reorientation of a free $BaTiO_3$ nanoparticle. Thus there is no clamping or its effect on the switching process is negligibly weak, and therefore, was not considered during the calculation.

IV. CONCLUSIONS

In summary, both 180° and 90° intrinsic polarization switching in $BaTiO_3$ crystal were investigated by LGD theory under uniaxial electromechanical loading. Results show that for 180° PS, it can be significantly influenced by stress. $E_{IC}^{180^\circ}$ increases under tension but decreases under compression with increasing stresses. For 90°, it was classified into two types. Similar to 180° intrinsic PS, $E_{IC}^{\text{I}\,(90^\circ)}$ increases under tension but decreases under compression with increasing stresses; while for the type II 90° PS, $E_{IC}^{\text{II}\,(90^\circ)}$ shows an opposite variation trend compared with $E_{IC}^{\text{I}\,(90^\circ)}$ and $E_{IC}^{180^\circ}$. Additionally, these calculations demonstrate that under tensile stresses or under compressive stresses in the range of −140 to 0 MPa, 90° PS is easier than 180° PS. As a result, 180° PS is prone to be accomplished by two-step 90° PS, which is inconsistent with the results observed in experiment. As E_{IC} refers to 180° PS in the past investigations, these demonstrate that the $E_{IC}^{180^\circ}$ calculated by others may be overestimated. Moreover, the coercive stress needed to drive 90° ferroelastic IPS was also

calculated. Results show that the stresses needed to drive the 90° ferroelastic DS are preloading electric fields dependent. $\sigma^{\mathrm{I}(90^\circ)}_{IC(P_3\rightarrow P_1/-P_1)}$ and $\sigma^{II(90^\circ)}_{IC(P_1/-P_1\rightarrow P_3)}$ decrease with increasing electric fields; while for $\sigma^{\mathrm{I}(90^\circ)}_{IC(-P_3\rightarrow P_1/-P_1)}$, it increases with increasing electric fields. Further, the effects of domain wall and depolarization energy on the polarization switching behavior were also estimated by phase field simulations. Results demonstrate that they have influences on PS in ferroelectrics, but are not critically important. These results were thought to be helpful for understanding the PS behavior in ferroelectrics.

ACKNOWLEDGMENTS

Y.L. acknowledges the support from the research foundation of Wuhan University and the NSF of China under Grant No. 11402177. F.L. acknowledges the support from the NSF of China under Grant No. 11422216.

[1] W. J. Merz, Phys. Rev. **95**, 690 (1954).
[2] E. A. Little, Phys. Rev. **98**, 978 (1955).
[3] S. V. Kalinin, S. Jesse, B. J. Rodriguez, Y. H. Chu, R. Ramesh, E. A. Eliseev, and A. N. Morozovska, Phys. Rev. Lett. **100**, 155703 (2008).
[4] S. Jesse, B. J. Rodriguez, S. Choudhury, A. P. Baddorf, I. Vrejoiu, D. Hesse, M. Alexe, E. A. Eliseev, A. N. Morozovska, J. Zhang, L. Q. Chen, and S. V. Kalinin, Nat. Mater. **7**, 209 (2008).
[5] P. Maksymovych, S. Jesse, M. Huijben, R. Ramesh, A. Morozovska, S. Choudhury, L. Q. Chen, A. P. Baddorf, and S. V. Kalinin, Phys. Rev. Lett. **102**, 017601 (2009).
[6] A. F. Devonshire, Philos. Mag. **40**, 1040 (1949).
[7] L. D. Laudau and E. M. Lifshitz, *Electrodynamics of Continuous Media* (Gostekhizdat, Moscow, 1957).
[8] J. F. Scott, Adv. Mater. **22**, 5315 (2010).
[9] R. Landauer, J. Appl. Phys. **28**, 227 (1957).
[10] S. Ducharme, V. M. Fridkin, A.V. Bune, S. P. Palto, L. M. Blinov, N. N. Petukhova, and S. G. Yudin, Phys. Rev. Lett. **84**, 175 (2000).
[11] A. M. Bratkovsky and A. P. Levanyuk, Phys. Rev. Lett. **87**, 019701 (2001).
[12] R. L. Moreira, Phys. Rev. Lett. **88**, 179701 (2002).
[13] N. A. Pertsev, J. Rodríguez Contreras, V. G. Kukhar, B. Hermanns, H. Kohlstedt, and R. Waser, Appl. Phys. Lett. **83**, 3356 (2003).
[14] M. J. Highland, T. T. Fister, M. I. Richard, D. D. Fong, P. H. Fuoss, C. Thompson, J. A. Eastman, S. K. Streiffer, and G. B. Stephenson, Phys. Rev. Lett. **105**, 167601 (2010).
[15] M. J. Highland, T. T. Fister, D. D. Fong, P. H. Fuoss, Carol Thompson, J. A. Eastman, S. K. Streiffer, and G. B. Stephenson, Phys. Rev. Lett. **107**, 187602 (2011).
[16] S. V. Kalinin, N. J. Rodriguez, S. Jesse, Y. H. Chu, T. Zhao, R. Ramesh, S. Choudhury, L. Q. Chen, E. A. Eliseev, and A. N. Morozovska. Proc. Natl. Acad. Sci. USA **104**, 20204 (2007).
[17] J. Wang and M. Kamlah, Phys. Rev. B **80**, 012101 (2009).
[18] T. Nakajima, R. Abe, Y. Takahashi, and T. Furukawa, Jpn. J. Appl. Phys. **44**, 1385 (2005).
[19] Y. W. Li, J. F. Scott, D. N. Fang, and F. X. Li, Appl. Phys. Lett. **103**, 232901 (2013).
[20] B. Jaffe, W. R. Cook, and H. Jaffe, *Piezoelectric Ceramics* (Academic, London, 1971).
[21] N. A. Pertsev, A. G. Zembilgotov, and A. K. Tagantsev, Phys. Rev. Lett. **80**, 1988 (1998).
[22] H. H. Wu, J. Z. Zhu, and T. Y. Zhang, Nano Energy **16**, 419 (2015).
[23] B. Jiang, Y. Bai, W. Y. Chu, Y. J. Su, and L. J. Qiao, Appl. Phys. Lett. **93**, 152905 (2008).
[24] Y. W. Li and F. X. Li, Appl. Phys. Lett. **104**, 042908 (2014).
[25] M. S. Senousy, R. K. N. D. Rajapakse, and M. S. Gadala, Acta. Mater. **57**, 6135 (2009).
[26] F. X. Li, D. N. Fang, and A. K. Soh, Smart. Mater. Struct. **13**, 668 (2004).
[27] S. V. Kalinin, A. N. Morozovska, L. Q. Chen, and B. J. Rodriguez, Rep. Prog. Phys. **73**, 056502 (2010).
[28] J. Hlinka and P. Márton, Phys. Rev. B **74**, 104104 (2006).
[29] P. Márton, I. Rychetsky, and J. Hlinka, Phys. Rev. B **81**, 144125 (2010).
[30] E. A. Eliseev, P. V. Yudin, S. V. Kalinin, N. Setter, A. K. Tagantsev, and A. N. Morozovska, Phys. Rev. B. **87**, 054111 (2013).
[31] A. N. Morozovska, E. A. Eliseev, Y. Li, S. V. Svechnikov, P. Maksymovych, V. Y. Shur, V. Gopalan, L.-Q. Chen, and S. V. Kalinin, Phys. Rev. B **80**, 214110 (2009).